



Experimental demonstration on detonation initiation by laser ignition and shock focusing in elliptical cavity

T. Sato¹ · K. Matsuoka¹ · A. Kawasaki² · N. Itouyama¹ · H. Watanabe³ · J. Kasahara¹

Received: 20 April 2023 / Revised: 11 October 2023 / Accepted: 12 October 2023 / Published online: 27 January 2024
© The Author(s) 2024, corrected publication 2024

Abstract

As a method of initiating detonation in a short distance with a small amount of energy, the combination of laser ignition and shock focusing in an elliptical cavity was proposed and experimentally demonstrated with a $C_2H_4-O_2$ mixture at 100 kPa and 297 K. In the experiment, an elliptical cavity and single rectangular cavities of different heights were used, and their flow-field patterns were visualized using high-speed schlieren imaging. Detonation initiation was achieved in the case of the elliptical cavity, and based on the Mach number change of the leading shock wave, two propagation phases were verified: the deceleration and acceleration phases. The deceleration phase was driven merely by the gasdynamic effect, wherein the initial shock wave (ISW) expanded spherically, and the acceleration phase began when the ISW shifted to planar propagation. In the acceleration phase, although gradual acceleration was observed in rectangular cavities, rapid acceleration occurred in the elliptical cavity. From the schlieren images, the second acceleration was caused not only by the concave reflected shock wave's catching up with the ISW, but also by the fast-flames that were generated along the cavity corners and engulfed the ISW in the converging section of the elliptical cavity.

Keywords Detonation initiation · Laser ignition · Shock focusing · Elliptical cavity · Schlieren imaging

1 Introduction

Detonation is a supersonic combustion that propagates at 2000–3000 m/s [1]. According to the ZND theory [2, 3], a detonation wave consists of a shock wave followed by chemical reactions. It is anticipated that detonation waves will be implemented in the propulsion systems of rockets and satellites [4], such as the Oblique Detonation Wave Engine

[5], Detonation-Driven Ramjet [6], Pulse Detonation Engine [7–9], and Rotating Detonation Engine [2, 10, 11], to make it possible to omit the compressors of the fuel and oxidizer [12], decrease the combustion-chamber length [13], hasten the thrust response [14], and increase the thermodynamic efficiency [15].

Conventionally, there are two methods for initiating detonations. The first one is deflagration-to-detonation transition (DDT), wherein a detonation wave is generated by local explosions behind accumulated compression waves that are emitted from a following combustion wave [16]. While DDT is advantageous owing to its low ignition energy of only a few milli-joules [17], a few hundred millimeters are necessary for

Communicated by G. Cicarelli.

This paper is based on work that was presented at the 29th International Colloquium on the Dynamics of Explosions and Reactive Systems, SNU Siheung, Korea, July 23–28, 2023.

✉ K. Matsuoka
matsuoka@nuae.nagoya-u.ac.jp

T. Sato
sato.tomoyuki.k1@s.mail.nagoya-u.ac.jp

A. Kawasaki
kawasaki.akira@shizuoka.ac.jp

N. Itouyama
itouyama@imass.nagoya-u.ac.jp

H. Watanabe
hiroaki.watanabe@ensma.fr

J. Kasahara
kasahara@nuae.nagoya-u.ac.jp

¹ Department of Aerospace Engineering, Nagoya University, Nagoya, Japan

² Department of Mechanical Engineering, Shizuoka University, Hamamatsu, Japan

³ Department Fluides, Thermique et Combustion, École Nationale Supérieure de Mécanique et d'Aérotechnique, Chasseneuil du Poitou, France

the flame kernel to turn into a detonation wave [18]. In contrast, the second method of direct detonation initiation (DDI) is capable of initiating detonations within a few millimeters [19]. However, DDI requires a few thousand milli-joules for successful initiation [20]. Therefore, taking into consideration the pros and cons of DDT and DDI, a new method that can initiate detonation waves in a short distance with a small amount of energy is now under investigation.

Several types of ignition have been proposed, such as an electrode or a spark plug [21], gunpowder [22], an exploding wire [23], laser irradiation [24], shock focusing [25], turbulent jet initiation [26], and a photochemical reaction [27]. Among these, the combination of laser ignition and shock focusing is expected to achieve the objective. In laser ignition, a high-power laser beam is focused into a reactive medium to initiate combustion [28], where laser beam is focused in a volume of 10–100 μm , the energy density reaches 10^{10} – 10^{11} W/cm^2 so that optical breakdown occurs, which generates plasma at the beam waist [29]. The plasma transforms into a flame kernel in 10–100 μs , which is used as the ignition source in general laser ignition process [30]. However, before this, owing to the plasma's rapid expansion, a spherical shock wave is generated in 10–100 ns [31], and it is expected that, by reflecting and converging the shock, a local explosion will occur, which works as a trigger for initiating detonation.

The potential of shock focusing in detonation initiation has been investigated theoretically, experimentally, and numerically to scrutinize the flow-field pattern and the distributions of pressure, temperature, velocity, etc. As a pioneering study, Voevodsky and Soloukhin [32] elucidated that detonation can be initiated behind the reflected shock with two ignition modes: strong and mild ignitions, which were then experimentally observed by Meyer and Oppenheim [33]. Borisov et al. [34] used spherical, cylindrical, conical, and planar reflectors to determine that non-planar reflectors diminish the ignition time and minimum incident shock Mach number. Similarly, Gelfand et al. [35] visualized the flow-field in the case of two-dimensional wedge, cylindrical, and parabolic reflectors such that detonation initiation occurred at different positions in the cases of mild and strong ignitions. Although these studies clarified that focusing can initiate detonation, as they were conducted using shock tubes, the incident shock was a planar one, which implies that there is little knowledge on the relation between spherical shock focusing and detonation initiation.

The combination of laser ignition and shock focusing is of interest from the perspectives of engineering and academics. Firstly, these two methods have a geometrical synergy because laser ignition can offer room for shock convergence without obstacles, in contrast to conventional spark-plug ignition. Secondly, as a spherical shock wave decays to a sonic wave in micro-seconds [36], its ignition

capability has not been suitably evaluated as a detonation initiator. Thus, if used effectively, the proposed method could be used to exploit the full potential of laser ignition. Finally, the detonability at the converging point can be higher than that in the case of planar shock focusing because a spherical shock results in a concave reflected shock and converges to a point, while a planar shock converges to a line.

The main objective of this study is to conduct laser ignition using shock focusing to demonstrate detonation initiation. Because ellipse is a geometry that the sum of the two distances to the focal points is constant on the curve, an elliptical reflector is suitable as a common geometry for converging a radially expanding wave [37–39]. Therefore, an elliptical cavity is used in the experiment and the flow-field is visualized using high-speed schlieren imaging such that the shock convergence and shock–flame interaction can be observed until the detonation initiation.

2 Experimental setup

2.1 Combustion chamber

Figure 1 presents the longitudinal cross section of the combustion chamber. The chamber is 60 mm long and 50 mm square in the transverse direction. There is a 23-mm-square hollow inside the chamber wherein a three-dimensionally printed cartridge with a cavity is inserted. The cartridge is of 3-mm thickness and is enclosed by three pairs of visualization windows fabricated using acrylic plate (PMMA), fused silica, and heat-resistant glass (TEMPAX Float). While an ellipsoid is favorable to heighten the shock-focusing effect, windows are installed to visualize the flow-field. There are a conical hole at the right end of the chamber for the ignition laser to enter, a 3-mm-diameter hole at the left end to calibrate the laser's direction, and a vertical hole at the top to fill and exhaust the mixture. The total pressure at the vertical hole is monitored using a low-speed pressure transducer (KELLER, PAA-23).

The various shapes of the cavities used are illustrated in Fig. 2 with their cross sections. The elliptical cavity is referred to as ELP in this study; the elliptical section has a 4-mm major radius and 2-mm minor radius and is connected to the rectangular section of 2-mm height. The other cavities do not comprise an elliptical section and are labeled as RCT2 and RCT4, where the number after RCT indicates the height of the cavity. The coordinate system described in Fig. 2 presents the center line of the cavities as the x -axis, which is used to analyze the change in Mach number. The origin is considered at the left end of the cavity, and the x -axis is considered to point toward the outlet of the cavity.

The cavity is filled with quiescent pre-mixed C_2H_4 – O_2 whose equivalence ratio is 1.0. The initial pressure and tem-

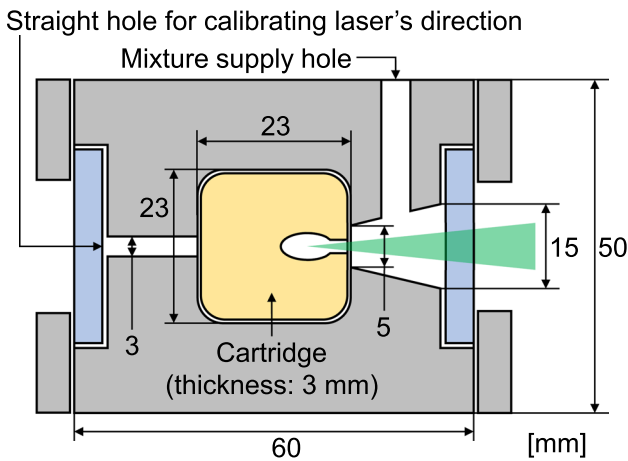


Fig. 1 Cross section of the combustion chamber. The ignition laser enters the cavity from the right

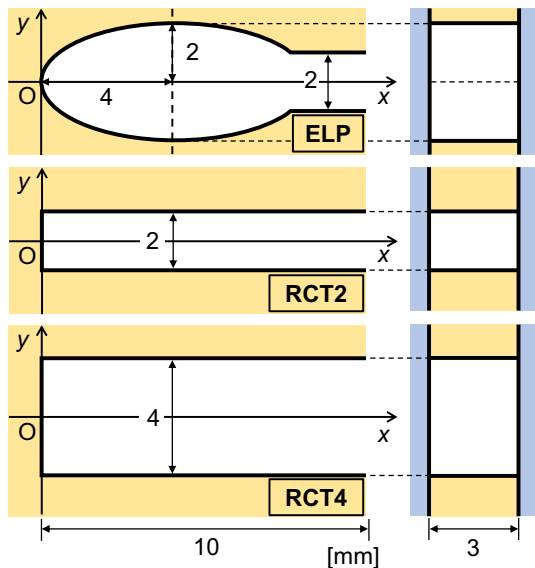


Fig. 2 Various cavities used in this study (left) and their cross sections (right), illustrated using the Cartesian coordinate system. The elliptic cavity is labeled ELP (top), and the rectangular cavities are labeled RCT2 (middle) and RCT4 (bottom)

perature for each case are as follows: in the case of ELP, $p_0 = 100 \text{ kPa}$ and $T_0 = 297 \text{ K}$; in the case of RCT2, $p_0 = 100 \text{ kPa}$ and $T_0 = 298 \text{ K}$; and in the case of RCT4, $p_0 = 101 \text{ kPa}$ and $T_0 = 298 \text{ K}$.

2.2 Optical systems

Figure 3 presents the optical systems for the laser ignition, which is described by green lines, and the one for schlieren visualization, which is described by red lines. For the ignition, a Nd:YAG laser system (New Wave Research, Tempest 10) is used to deliver a single pulsed laser beam with an irradiation energy of $195 \pm 3 \text{ mJ}$ at a wavelength

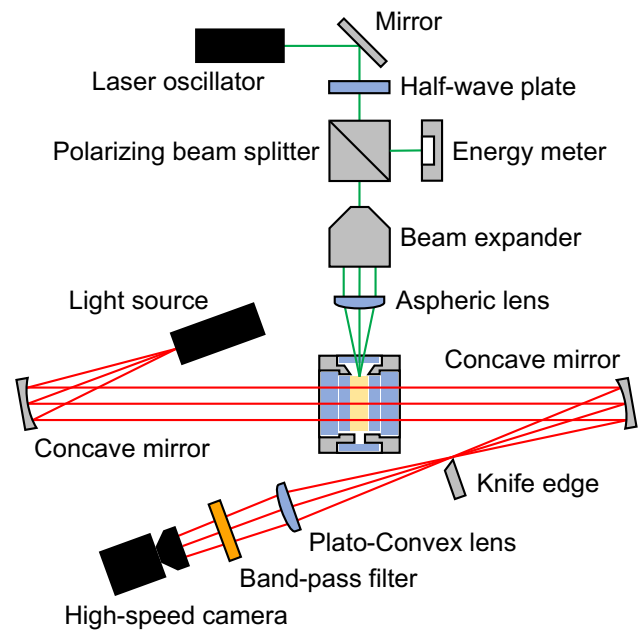
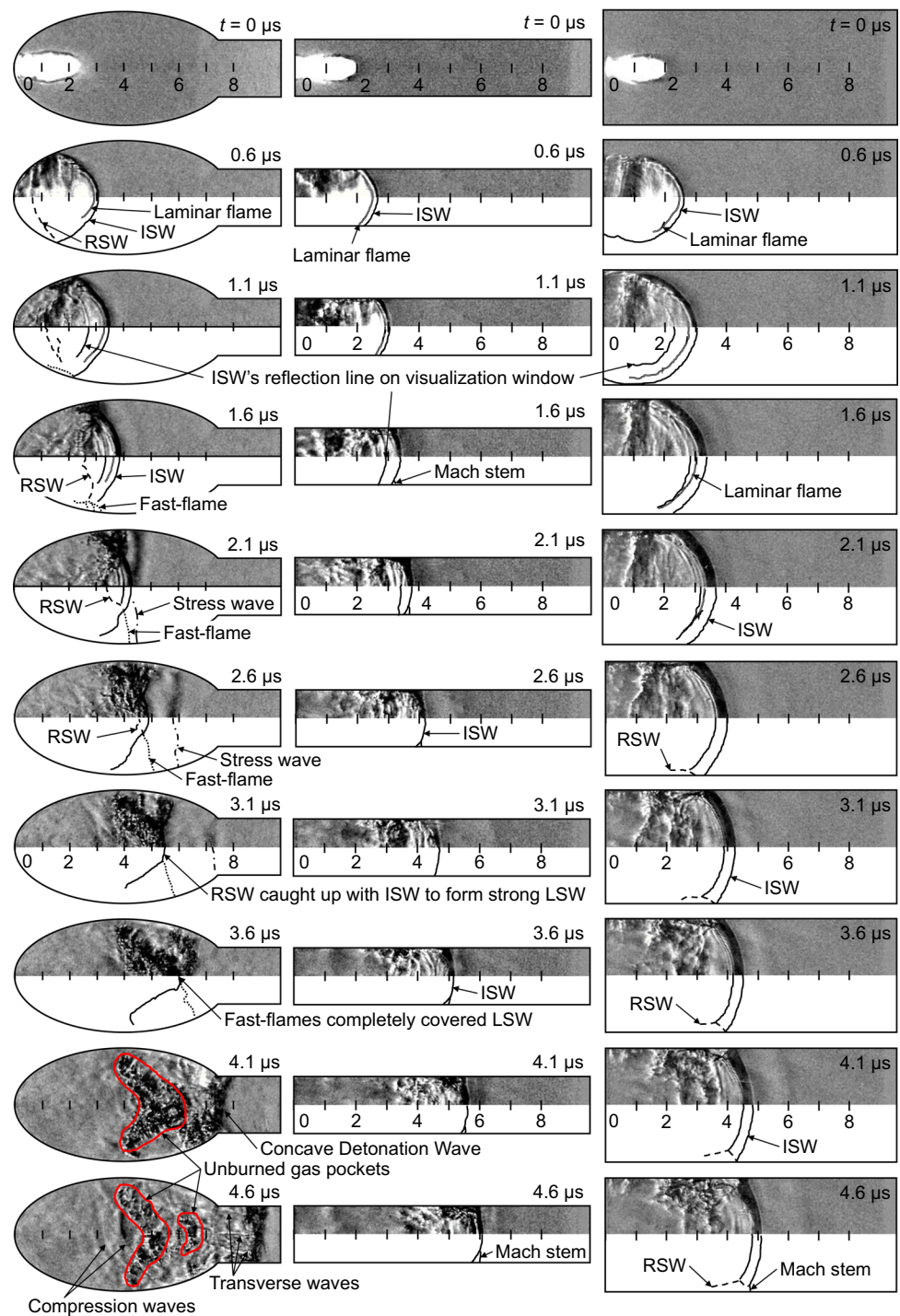


Fig. 3 Top view of the optical systems: the optical system for laser ignition (green) and for schlieren visualization (red)

of 1064 nm and full width at half maximum pulse length of $5.0 \pm 0.3 \text{ ns}$. The laser passes through a half-wave plate and a polarizing beam splitter, and one of the split beams is delivered to an energy detector (Gentec-EO, QE25LP-H-MB-QED-INT). The diameter of the other beam is amplified from 5 to 15 mm using a beam expander and then focused using a plato-convex lens with a focal length of 75 mm. The ignition laser is focused at $x = 0.5 \text{ mm}$, which corresponds to the left focal point of ELP in Fig. 2. The focal point in transverse direction is 1.5 mm away from the visualization windows so that the spherical shock wave reaches the cavity's left wall before reaching the other walls and forms one concave reflected shock wave. According to a previous study conducted by Kojima et al. [40], the energy absorption rate of incident laser beam is approximately 50% in air at a pressure of 0.1 MPa.

For high-speed schlieren imaging, a pulsed diode laser light source (Cavitar, Cavilux Smart UHS 50W) provides a repetitive pulsed laser at $644 \pm 10 \text{ nm}$ for a 20-ns pulse length. A pair of concave mirrors having a focal length of 500 mm is used to obtain a parallel light, and a plato-convex lens having a focal length of 1500 mm is used along with a 640-nm band-pass filter, which removes chemical luminescence from the combustion wave, in front of the high-speed camera (Shimadzu, HPV-X2). The exposure time of the camera is 50 ns, and the recording is conducted with a frame rate of 100 ns per frame.

Fig. 4 Sequential schlieren images (upper half) and their sketches (lower half) of the flow-field in ELP (left), RCT2 (center), and RCT4 (right). The time $t = 0$ is when the plasma luminescence was observed



3 Results and discussion

3.1 Overall flow-field features

Figure 4 presents the sequential schlieren images and sketches of the flow-field. In order to remove the static noises, each image was generated by taking average of the original image and the inverted pre-ignition image. First, an elliptical plasma

kernel was observed as reported by Chen et al. [41], and the plasma kernel formed an elliptical initial shock wave (ISW) followed by a laminar flame at $t = 0.6 \mu\text{s}$. Exclusively in ELP, a concave reflected shock wave (RSW) was also formed because of the round cavity left end wall [42]. Owing to the induced flow behind the ISW and the concave-shaped RSW, the RSW had got closer to the ISW over time [43]. At $t = 1.1\text{--}1.6 \mu\text{s}$, when the ISW reflected

on the visualization window, the reflection point appeared as a curve because the ISW had a round shape. After $t = 1.6 \mu\text{s}$, while gradual flame acceleration occurred in RCT2 and RCT4, fast-flame was generated near the upper and lower cavity walls of ELP and started to engulf the ISW. The interaction point between the ISW and the fast-flame moved toward the center line from upper and lower cavity walls. In addition, stress waves were also observed in front of the fast-flame near the cavity walls. At $t = 3.1 \mu\text{s}$ ($x = 5.5 \text{ mm}$), the RSW caught up with the ISW to form a strong leading shock wave (LSW), and the fast-flame completely covered the LSW at $t = 3.6 \mu\text{s}$ ($x = 6.0 \text{ mm}$). A concave detonation wave was observed at $t = 4.1 \mu\text{s}$, and it deformed into a planar one in the rectangular section with three transverse waves at $t = 4.6 \mu\text{s}$. A bow-shaped regime was also observed, which then separated into two parts. The regime originally located along the ISW, which was behind the fast-flames at $t = 3.1\text{--}4.1 \mu\text{s}$ in ELP. And, as to be discussed in Sect. 3.4, considering that the fast-flames were generated at the four cavity corners, the unburned gas at the cavity center would be taken into at last. Because schlieren imaging visualizes the density gradient and the bow-shaped regime located behind the detonation eventually, the regime was considered as an unburned gas pocket.

The history of LSW's position along the center line was displayed as an x - t diagram in Fig. 5. In all cases, the ISW propagated in the positive x -direction in the initial stage as observed in Fig. 4. Then, a line indicating the RSW appeared at $t = 1.0 \mu\text{s}$ in ELP, whereas such a line was not observed in RCT2 and RCT4. Given that the ISW was observed in RCT2 and RCT4 and that these cavities have a planar left end wall, there should have been a convex RSW [44]. However, as such RSW was not observed as shown in Figs. 4 and 5, it was considered that the RSW was not strong and would not form a strong LSW in RCT2 and RCT4. Next, a new wave appeared in front of the ISW, for example at $t = 2.1 \mu\text{s}$ ($x = 4.3 \text{ mm}$) in ELP. The velocity was $2844 \pm 284 \text{ m/s}$, and as the speed of sound in PMMA is 2735 m/s [45], it could be presumed that this wave was a stress wave propagating in the visualization window. As to be discussed in detail in Sect. 3.4, it was speculated that the interaction of shock waves along the cavity corner caused a locally high-pressure regime and pressurized the window, which would be visualized as a stress wave. In ELP, the inclination of the ISW decreased at $x = 6.0 \text{ mm}$ where the RSW line caught up with the ISW line, and an overdriven detonation wave propagating at $2951 \pm 295 \text{ m/s}$ was then confirmed.

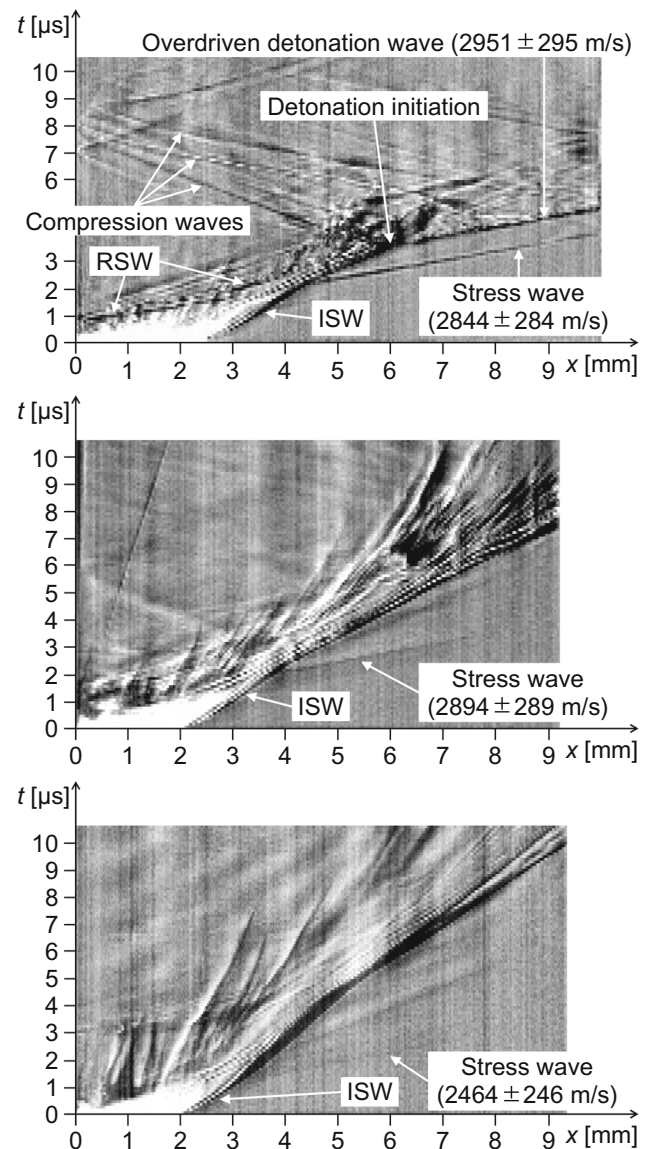


Fig. 5 Time–displacement diagrams at the center line of ELP (top), RCT2 (middle), and RCT4 (bottom). The displacement $x = 0$ is at the cavity's left end, and $t = 0$ is set as the time when the plasma luminescence was observed. The velocities of the overdriven detonation wave and stress wave were calculated from their inclinations in the figure

3.2 Deceleration phase

From Fig. 5, the position of the LSW, including ISW and detonation wave, was determined. And, after taking moving average of 5 points, the Mach number of the LSW on the x -axis, M_x , was calculated using the following equation:

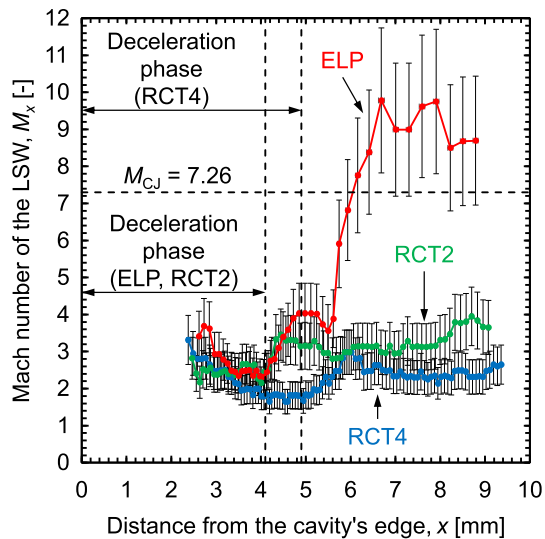


Fig. 6 Mach number of the LSW on the x -axis, M_x , versus the displacement, x . The initial pressure and temperature for each case are as follows: for ELP, $p_0 = 100$ kPa and $T_0 = 297$ K; for RCT2, $p_0 = 100$ kPa and $T_0 = 298$ K; and for RCT4, $p_0 = 101$ kPa and $T_0 = 298$ K

$$M_x = \frac{dx/dt}{a_0} \quad (1)$$

where a_0 is the speed of sound of the unburned gas in front of the LSW calculated by NASA-CEA code [46, 47] with the initial pressure and temperature, p_0 and T_0 . The Mach number in three cavities was compared in Fig. 6, and in spite of the cavity shape difference, the Mach number change could broadly be classified into two phases: deceleration and acceleration.

The average of initial Mach number among three cases was $M_x = 3.18 \pm 0.26$; however, it decreased to $M_x = 2.05 \pm 0.28$ at $x = 4.1$ mm in ELP and RCT2 and at $x = 4.9$ mm in RCT4. Considering that the deceleration phase was common in all cavities and that the initial ISW propagated spherically, the expansion regime behind the spherical ISW had a significant effect on the decrease in Mach number. Given that the curvature of the ISW was small at $x = 4.1$ mm in ELP and RCT2 compared to that in RCT4, the ISW's shift from spherical propagation to planar propagation became the end of the deceleration phase. This result was similar to the description by Yageta et al. [48] on the flame deformation in DDT when igniting near the end of a shock tube.

3.3 Acceleration phase

After the deceleration phase, the Mach number increased in all cavities. While RCT2 and RCT4 experienced gradual acceleration, ELP had a two-staged acceleration. The

first acceleration occurred at $x = 4.1$ mm reaching $M_x = 4.0$ where the ISW shifted from spherical propagation to planar propagation. The second acceleration occurred at $x = 5.5$ mm, which corresponds to the moment when the RSW caught up with ISW to form a strong LSW in Fig. 4. Furthermore, as the fast-flame engulfed the LSW to form a concave detonation wave in the converging section of ELP, the geometrical features of detonation wave and cavity also helped the second acceleration [43, 49]. The Mach number eventually reached $M_x = 9.8$ indicating that an overdriven detonation was initiated. After $x = 6.7$ mm, the Mach number started to decrease gradually forming a planar self-sustained detonation wave eventually.

In the other cases, such as in RCT2, although the Mach number increased at the same location as that in ELP, it kept constant at $M_x = 3.1$. Although it increased again at $x = 8.0$ mm, gradual flame acceleration occurred afterward as mentioned in Sect. 3.1. RCT4 had the same Mach number change although the maximum value was $M_x = 2.3$, which was lower than that in RCT2. This was because the cavity height of RCT4 is larger than the others, and the ISW traveled a longer distance before shifting to planar propagation resulting in greater decay and lower Mach number.

3.4 Detailed flow-field features before detonation onset

Based on the schlieren images, $x-t$ diagrams, and Mach number changes, it is considered that there were mainly two factors for the detonation onset: the concave RSW's catching up with the ISW to form a strong LSW and the fast-flame's engulfing the LSW. As for the RSW, it originated in the elliptical curve of the cavity's end wall; however, as for the fast-flame, it is still not clear where the fast-flame was generated and how it propagated. Figure 7 presents the images before and after the fast-flame generation in higher temporal resolution. The fast-flame was observed near the lower cavity wall at $t = 1.0$ μ s and by the upper cavity wall at $t = 1.1$ μ s. Because schlieren images present the flow-field two-dimensionally, given that the ISW propagated three-dimensionally, it is indispensable to have three-dimensional understanding of the flow-field to clarify where the fast-flame was generated. Thus, a mock flow-field was made using a three-dimensional computer-aided design (3D CAD) software presented in Fig. 8. Although the visualization windows are not displayed in the figure, ISW had two reflections: one is on the cavity wall, observed as RSW, and the other is on the visualization windows, observed as reflection line. In addition, as for the RSW, Mach reflection could occur as shown in Appendix. From Fig. 8, the fast-flame appeared at the interaction point of RSW and ISW's reflection line. Because the interaction point is where ISW's two reflected shock waves passed through, it could have higher pressure and

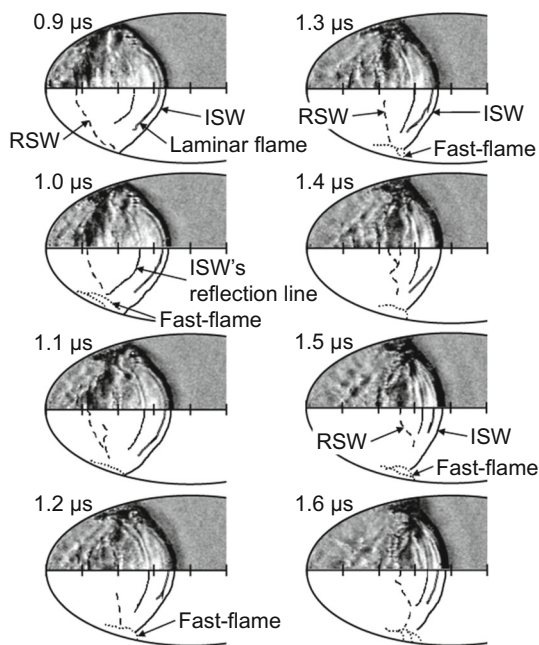


Fig. 7 Sequential schlieren images (upper half) and their sketches (lower half) of the flow-field in ELP before and after the fast-flame generation. The time $t = 0$ is when the plasma luminescence was observed

temperature than at the cavity center [50–52]. High-pressure regime near the visualization window would result in a stress wave as observed in Fig. 4. Considering that the laminar flame behind the ISW also reached the cavity wall and the visualization window, an auto-ignition would also occur along the cavity corner, resulting in fast-flame generation. However, more importantly, this type of shock reflections in 90-degree corner could also occur in RCT2 and RCT4. Therefore, the fast-flame originated in the shock interaction phenomenon was a less dominant factor for the detonation onset than the concave RSW catching up with the ISW.

After the fast-flame generation, it propagated engulfing the ISW as presented in Fig. 9. As there are four corners in the cavity (two at the top and two at the bottom of the cavity as described in the right side of Fig. 2), the fast-flame engulfed the ISW from these four corners. The interaction point between the flame and the cavity wall was traced in the schlieren images so that the velocity of these flames was calculated as shown in Fig. 10. Because the velocity varied from 50 to 90% of the CJ detonation speed, a coupling of the ISW and the fast-flame, referred as “turbulent shock-flame complex” [53–55], occurred.

4 Conclusion

The combination of laser ignition and shock focusing was proposed as a new method of initiating a detonation using

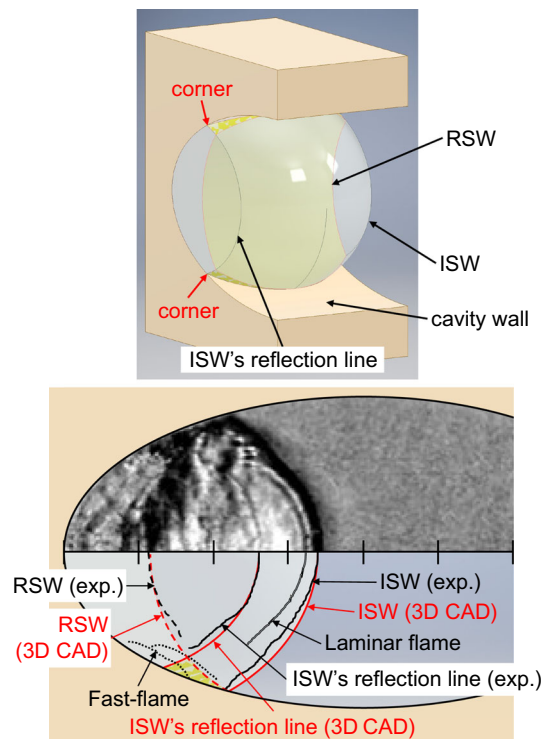


Fig. 8 Overall view of the mock flow-field (top) and the comparison with schlieren image from the side view at $t = 1.0 \mu s$ (bottom). In the comparison, the flow-field sketch is displayed in black and mock flow-field is displayed in red

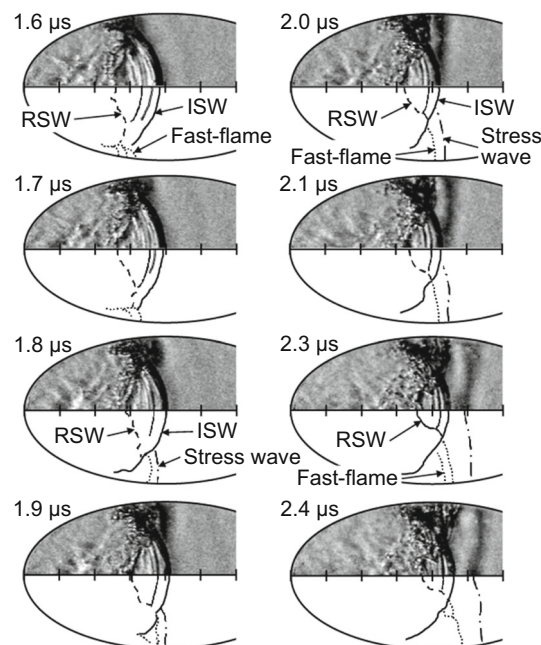


Fig. 9 Sequential schlieren images (upper half) and their sketches (lower half) of the flow-field in ELP during fast-flame engulfing the ISW. The time $t = 0$ is when the plasma luminescence was observed

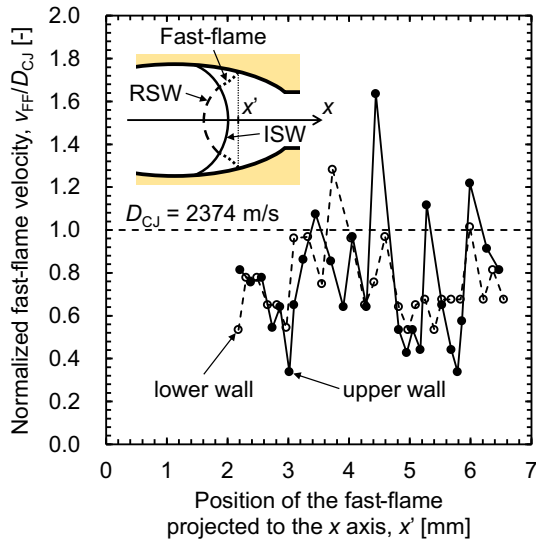


Fig. 10 Velocities of fast-flame normalized by the CJ detonation speed, v_{FF}/D_{CJ} , versus their position projected to the x -axis, x' . Closed symbol indicates the normalized velocity of the fast-flame at the upper cavity wall, and open symbol indicates the one at the lower cavity wall

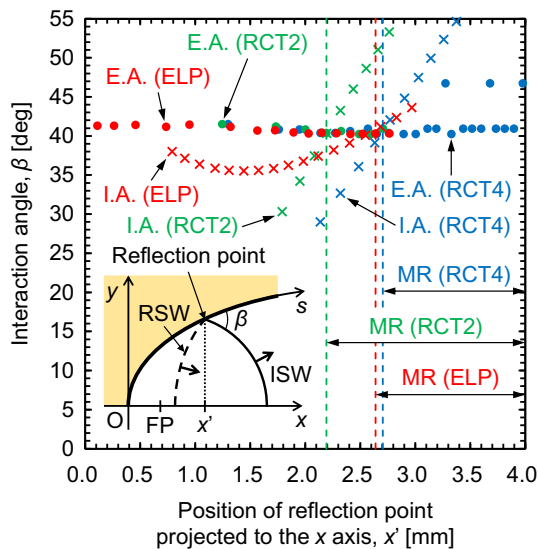


Fig. 11 Comparison of the extreme angles (E.A.) at upper wall (closed circle) and lower wall (open circle) and the interaction angle (I.A.) between the ISW and cavity wall (cross symbol) in ELP (red), RCT2 (green), and RCT4 (blue). The horizontal axis, x' , shows the position of the reflection point projected to the x -axis. The broken lines indicate where RR turns into MR

a small amount of energy in a short distance. Experiments were conducted using an elliptical cavity (ELP) and two rect-

angular cavities of different heights (RCT2 and RCT4) with a stoichiometric $C_2H_4-O_2$ mixture at a pressure of 100 kPa and temperature of 297 K.

First, the flow-field inside the cavity was visualized using high-speed schlieren imaging. An overdriven detonation wave was observed in ELP, and gradual flame acceleration was observed in RCT2 and RCT4.

Second, the Mach number change at the center line of each cavity was investigated, and it was verified that there were primarily two common phases for the propagation of the leading shock wave (LSW): the deceleration and acceleration phases. The deceleration phase lasted, while the initial shock wave (ISW) propagated spherically, and when it shifted to the planar propagation, the acceleration phase began. Although RCT2 and RCT4 exhibited a gradual flame acceleration, ELP exhibited a rapid acceleration to achieve overdriven detonation onset at the point where the concave reflected shock wave (RSW) caught up with the ISW to form a strong LSW.

Third, from the temporally more resolved schlieren images, the generation and propagation of fast-flames were investigated. As a result, it was indicated that the fast-flame was generated along the cavity corner where the reflected shock waves on the cavity wall and on the visualization window interact. Then, fast-flame propagated engulfing the ISW at 50% to 90% of the CJ detonation speed owing to the shock-flame interaction.

Based on these investigations, the detonation was initiated via the following scenario:

1. In ELP, the ISW was formed owing to the plasma kernel's rapid expansion.
2. The ISW reflected at the cavity end to form a concave RSW.
3. Fast-flames were generated along the four cavity corners and propagated engulfing the ISW.
4. The RSW caught up with the ISW to form a strong LSW.
5. Fast-flames completely covered up the LSW.
6. The fast-flame coupled with the LSW accelerated in the converging section to form a concave overdriven detonation wave.

As the generation and propagation of ISW, RSW, fast-flame, and detonation onset in realistic flow-field are complicated, three-dimensional simulations should be conducted in future study. In addition, chemical luminescence observation and pressure measurement along the cavity wall are also needed for more quantitative confirmation of the detonation.

Appendix

This appendix presents an estimation of the point where the ISW’s reflection mode changes from regular reflection (RR) to Mach reflection (MR). While the following analysis was conducted based on two-dimensional understanding of the flow-field, it is still helpful to predict if a Mach stem could be generated and work as one of the factors contributing the fast-flame generation and propagation.

In order to estimate the transition point, first, the coordinates of the reflection point were obtained from every schlieren image to calculate the interaction angle between the ISW and contour of ELP, β , using the following equations:

$$\beta = \arctan\left(-\frac{b^2 x_r - a}{a^2 y_r}\right) - \arctan\left(-\frac{d^2 x_r - f}{c^2 y_r}\right) \tag{2}$$

$$f = a - \sqrt{a^2 - b^2} \tag{3}$$

where (x_r, y_r) are the coordinates of the reflection point; a and b are the major and minor radii of ELP, respectively; and c and d are those of the ISW, respectively. The ISW was assumed to have its center $(f, 0)$ at the focal point of ELP. Next, for the comparison with the interaction angle, the extreme angle of the detachment criterion of two-shock theory [56] was considered. As described in Fig. 11, the s -axis was defined as that along the contour of ELP, and the apparent Mach number of the ISW along the s -axis was calculated using the following equation:

$$M_s = \frac{\sqrt{(\Delta x_r)^2 + (\Delta y_r)^2}}{a_0 \Delta t} \tag{4}$$

Assuming that the calculated regime was sufficiently close to the contour that the curvature of ELP, ISW, and RSW could be neglected, the extreme angle could be derived based on the two-shock theory as the maximum interaction angle satisfying the following equations:

$$\Pi_{ISW} = \frac{2\gamma_0 M_s^2 \sin^2 \beta}{\gamma_0 + 1} - \frac{\gamma_0 - 1}{\gamma_0 + 1} \tag{5}$$

$$\Pi_{RSW} = \frac{2\gamma_0 M_{RSW}^2 \sin^2(\alpha + \theta_{RSW})}{\gamma_0 + 1} - \frac{\gamma_0 - 1}{\gamma_0 + 1} \tag{6}$$

$$M_{RSW} = \frac{1}{\sin(\beta - \theta_{ISW})} \sqrt{\frac{(\gamma_0 - 1) M_s^2 \sin^2 \beta + 2}{2\gamma_0 M_s^2 \sin^2 \beta - (\gamma_0 - 1)}} \tag{7}$$

$$\theta_{ISW} = \arctan\left(\frac{\Pi_{ISW} - 1}{1 + \gamma_0 M_s^2 - \Pi_{ISW}} \sqrt{\frac{\frac{2\gamma_0 M_s^2}{\gamma_0 + 1} - \frac{\gamma_0 - 1}{\gamma_0 + 1} - \Pi_{ISW}}{\Pi_{ISW} + \frac{\gamma_0 - 1}{\gamma_0 + 1}}}\right) \tag{8}$$

$$\theta_{RSW} = \arctan\left(\frac{\Pi_{RSW} - 1}{1 + \gamma_0 M_{RSW}^2 - \Pi_{RSW}} \sqrt{\frac{\frac{2\gamma_0 M_{RSW}^2}{\gamma_0 + 1} - \frac{\gamma_0 - 1}{\gamma_0 + 1} - \Pi_{RSW}}{\Pi_{RSW} + \frac{\gamma_0 - 1}{\gamma_0 + 1}}}\right) \tag{9}$$

where Π_{ISW} and Π_{RSW} are the pressure amplitudes of the ISW and the RSW, respectively; γ_0 is the specific heat ratio of the unburned gas before the ISW at initial state calculated by NASA-CEA code [46, 47]; M_{RSW} is the Mach number of the flow entering the RSW; θ_{ISW} and θ_{RSW} are the deflection angles of the flow behind the ISW and the RSW, respectively; and α is the reflected angle of the RSW. Finally, to obtain the relation between the s and x coordinates, the following equations were used:

$$s = a \int_0^\phi \sqrt{1 - \frac{a^2 - b^2}{a^2} \sin^2 \psi} d\psi \tag{10}$$

$$\phi = \arccos\left(\frac{a - x_r}{a}\right) \tag{11}$$

Consequently, the interaction angle between the ISW and contour of ELP, β , was compared with the extreme angle, as shown in Fig. 11. According to the detachment criterion, once the interaction angle exceeds the extreme angle, the RR turns into MR. In Fig. 11, the transition occurred at $x' = 2.6$ mm. The calculated transition point roughly matched the one at which the fast-flame was observed for the first time in Fig. 4 or in Fig. 7. The Mach stem not only heightens the unburned gas temperature to shorten the reaction induction time, but also produces vortices to foster unburned/burned gas mixing as well as to produce forward jet [57]. It was also speculated that the “turbulent shock–flame complex” [53–55] occurred owing to the coupling of the Mach stem and flames.

Acknowledgements This work was supported by a JSPS Grant-in-Aid for Challenging Research (Exploratory) [Grant Number JP20K21046]. The author would also like to take this opportunity to thank the “Nagoya University Interdisciplinary Frontier Fellowship” supported by Nagoya University and JST, the establishment of university fellowships toward the creation of science technology innovation [Grant Number JPMJFS2120].

Funding Open Access funding enabled and organized by Projekt DEAL.

Open Access This article is licensed under a Creative Commons Attribution 4.0 International License, which permits use, sharing, adaptation, distribution and reproduction in any medium or format, as long as you give appropriate credit to the original author(s) and the

source, provide a link to the Creative Commons licence, and indicate if changes were made. The images or other third party material in this article are included in the article's Creative Commons licence, unless indicated otherwise in a credit line to the material. If material is not included in the article's Creative Commons licence and your intended use is not permitted by statutory regulation or exceeds the permitted use, you will need to obtain permission directly from the copyright holder. To view a copy of this licence, visit <http://creativecommons.org/licenses/by/4.0/>.

References

- Wolański, P.: Detonative propulsion. *Proc. Combust. Inst.* **34**, 125–158 (2013). <https://doi.org/10.1016/j.proci.2012.10.005>
- Zel'dovich, Y.B.: On the use of detonative combustion in power engineering. *J. Tech. Phys.* **10**(17), 1453–1461 (1940). Also see: Zel'dovich, Y.B.: To the question of energy use of detonation combustion. *J. Propuls. Power* **22**(3), 588–592 (2006). <https://doi.org/10.2514/1.22705>
- Fickett, W., Davis, W.C.: *Detonation: Theory and Experiment*. University of California Press, Berkeley (1979)
- Kailasanath, K.: Review of propulsion applications of detonation waves. *AIAA J.* **38**(9), 1698–1708 (2000). <https://doi.org/10.2514/2.1156>
- Menees, G.P., Adelman, H.G., Cambier, J.-L., Bowles, J.V.: Wave combustors for trans-atmospheric vehicles. *J. Propuls. Power* **8**(3), 709–713 (1992). <https://doi.org/10.2514/3.23536>
- Hertzberg, A., Bruckner, A.P., Bogdanoff, D.W.: Ram accelerator: a new chemical method for accelerating projectile to ultrahigh velocities. *AIAA J.* **26**(2), 195–203 (1988). <https://doi.org/10.2514/3.9872>
- Nicholls, J.A., Wilkinson, H.R., Morrison, R.B.: Intermittent detonation as a thrust-producing mechanism. *Jet Propuls.* **27**(5), 534–541 (1957). <https://doi.org/10.2514/8.12851>
- Bussing, T.R.A., Pappas, G.: An introduction to pulse detonation engines. 32nd Aerospace Sciences Meeting and Exhibit, Reno, NV, AIAA Paper 1994-263 (1994). <https://doi.org/10.2514/6.1994-263>
- Buyakofu, V., Matsuoka, K., Matsuyama, K., Kawasaki, A., Watanabe, H., Itouyama, N., Goto, K., Ishihara, K., Noda, T., Kasahara, J., Matsuo, A., Funaki, I., Nakata, D., Uchiumi, M., Habu, H., Takeuchi, S., Arakawa, S., Masuda, J., Maehara, K., Nakao, T., Yamada, K.: Flight demonstration of pulse detonation engine using sounding rocket S-520-31 in space. *J. Spacecr. Rocket.* **60**(1), 181–189 (2023). <https://doi.org/10.2514/1.A35394>
- Voitsekhovskii, B.V.: Stationary spin detonation. *Sov. J. Appl. Mech. Tech. Phys.* **3**, 157–164 (1960)
- Goto, K., Matsuoka, K., Matsuyama, K., Kawasaki, A., Watanabe, H., Itouyama, N., Ishihara, K., Buyakofu, V., Noda, T., Kasahara, J., Matsuo, A., Funaki, I., Nakata, D., Uchiumi, M., Habu, H., Takeuchi, S., Arakawa, S., Masuda, J., Maehara, K., Nakao, T., Yamada, K.: Space flight demonstration of rotating detonation engine using sounding rocket S-520-31. *J. Spacecr. Rocket.* **60**(1), 273–285 (2023). <https://doi.org/10.2514/1.A35401>
- Nettleton, M.A.: *Gaseous Detonations: Their Nature, Effects and Control*. Springer, Dordrecht (1987). <https://doi.org/10.1007/978-94-009-3149-7>
- Connolly-Boutin, S., Joseph, V., Ng, H.D., Kiyanda, C.B.: Small-size rotating detonation engine: scaling and minimum mass flow rate. *Shock Waves* **31**, 665–674 (2021). <https://doi.org/10.1007/s00193-021-00991-2>
- Matsuoka, K., Taki, H., Kasahara, J., Watanabe, H., Matsuo, A., Endo, T.: Pulse detonation cycle at kilohertz frequency. In: Li, J.-M., Teo, C.J., Khoo, B.C., Wang, J.-P., Wang, C. (eds.) *Detonation Control for Propulsion: Shock Wave and High Pressure Phenomena*, pp. 183–198. Springer, Cham (2018). https://doi.org/10.1007/978-3-319-68906-7_8
- Shepherd, J.E., Wintenberger, E.: Thermodynamic analysis of combustion processes for propulsion systems. 42nd AIAA Aerospace Sciences Meeting and Exhibit, Reno, NV, AIAA Paper 2004-1033 (2004). <https://doi.org/10.2514/6.2004-1033>
- Urtiew, P.A., Oppenheim, A.K.: Experimental observations of the transition to detonation in an explosive gas. *Proc. R. Soc. Lond. A* **295**(1440), 13–28 (1966). <https://doi.org/10.1098/rspa.1966.0223>
- Lim, E.H., McIlroy, A., Ronney, P.D., Syage, J.A.: Detailed characterization of minimum ignition energies of combustible gases using laser ignition sources. In: Chan, S.H. (ed.) *Transport Phenomena in Combustion: Proceedings of the 8th International Symposium on Transport Phenomena in Combustion*, pp. 176–184. Taylor & Francis, Washington (1996)
- Bollinger, L.E., Michael, C.F., Rudolph, E.: Experimental measurements and theoretical analysis of detonation induction distances. *ARS J.* **31**(5), 588–595 (1961). <https://doi.org/10.2514/8.5567>
- Bach, G.G., Knystautas, R., Lee, J.H.S.: Direct initiation of spherical detonation in gaseous explosives. *Symp. (Int.) Combust.* **12**, 853–864 (1969). [https://doi.org/10.1016/S0082-0784\(69\)80466-2](https://doi.org/10.1016/S0082-0784(69)80466-2)
- Lee, J.H.S., Matsui, H.: A comparison of the critical energies for direct initiation of spherical detonations in acetylene-oxygen mixtures. *Combust. Flame* **28**, 61–66 (1977). [https://doi.org/10.1016/0010-2180\(77\)90008-6](https://doi.org/10.1016/0010-2180(77)90008-6)
- Raizer, Y.P.: *Gas Discharge Physics*. Springer, Heidelberg (1991)
- Blackwood, J.D., Bowden, F.P.: The initiation, burning and thermal decomposition of gunpowder. *Proc. R. Soc. Lond. A* **213**(1114), 285–306 (1952). <https://doi.org/10.1098/rspa.1952.0127>
- Edwards, D.H., Hooper, G., Morgan, J.M., Thomas, G.O.: The quasi-steady regime in critically initiated detonation waves. *J. Phys. D Appl. Phys.* **11**(15), 2103–2117 (1978). <https://doi.org/10.1088/0022-3727/11/15/008>
- Lee, J.H.S., Knystautas, R.: Laser spark ignition of chemically reactive gases. *AIAA J.* **7**(2), 312–317 (1969). <https://doi.org/10.2514/3.5091>
- Bartenev, A.M., Khomik, S.V., Gelfand, B.E., Grönig, H., Olivier, H.: Effect of reflection type on detonation initiation at shock-wave focusing. *Shock Waves* **10**(3), 205–215 (2000). <https://doi.org/10.1007/s001930050008>
- Carnasciali, F., Lee, J.H.S., Knystautas, R., Fineschi, F.: Turbulent jet initiation of detonation. *Combust. Flame* **84**(1–2), 170–180 (1991). [https://doi.org/10.1016/0010-2180\(91\)90046-E](https://doi.org/10.1016/0010-2180(91)90046-E)
- Lee, J.H.S., Knystautas, R., Yoshikawa, N.: Photochemical initiation of gaseous detonations. *Acta Astronaut.* **5**(11–12), 971–982 (1978). [https://doi.org/10.1016/0094-5765\(78\)90003-6](https://doi.org/10.1016/0094-5765(78)90003-6)
- Ronney, P.D.: Laser versus conventional ignition of flames. *Opt. Eng.* **33**(2), 510–521 (1994). <https://doi.org/10.1117/12.152237>
- Morgan, C.G.: Laser-induced breakdown of gases. *Rep. Prog. Phys.* **38**(5), 621–665 (1975). <https://doi.org/10.1088/0034-4885/38/5/002>
- Spiglanin, T.A., McIlroy, A., Fournier, E.W., Cohen, R.B., Syage, J.A.: Time-resolved imaging of flame kernels: laser spark ignition of H₂/O₂/Ar Mixtures. *Combust. Flame* **102**(3), 310–328 (1995). [https://doi.org/10.1016/0010-2180\(94\)00278-Z](https://doi.org/10.1016/0010-2180(94)00278-Z)
- Korobkin, V.V., Mandel'shtam, S.L., Pashinin, P.P., Prokhideev, A.V., Prokhorov, A.M., Sukhodrev, N.K., Shchelev, M.Y.: Investigation of the air “spark” produced by focused laser radiation. III. *Sov. J. Exp. Theor. Phys.* **26**(1), 79–85 (1968)
- Voevodsky, V.V., Soloukhin, R.I.: On the mechanism and explosion limits of hydrogen-oxygen chain self-ignition in shock waves. *Symp. (Int.) Combust.* **10**(1), 279–283 (1965). [https://doi.org/10.1016/S0082-0784\(65\)80173-4](https://doi.org/10.1016/S0082-0784(65)80173-4)
- Meyer, J.W., Oppenheim, A.K.: On the shock-induced ignition of explosive gases. *Symp. (Int.) Combust.* **13**(1), 1153–1164 (1971). [https://doi.org/10.1016/S0082-0784\(71\)80112-1](https://doi.org/10.1016/S0082-0784(71)80112-1)

34. Borisov, A.A., Zamanskii, V.M., Kosenkov, V.V., Lisyanskii, V.V., Skachkov, G.I., Troshin, K.Y., Gelfand, B.E.: Ignition of gaseous combustible mixtures in focused shock waves. *AIP Conf. Proc.* **208**(1), 696–701 (1990). <https://doi.org/10.1063/1.39506>
35. Gelfand, B.E., Khomik, S.V., Bartenev, A.M., Medvedev, S.P., Grönig, H., Olivier, H.: Detonation and deflagration initiation at the focusing of shock waves in combustible gaseous mixture. *Shock Waves* **10**, 197–204 (2000). <https://doi.org/10.1007/s001930050007>
36. Phuoc, T.X.: Laser-induced spark ignition fundamental and applications. *Opt. Lasers Eng.* **44**(5), 351–397 (2006). <https://doi.org/10.1016/j.optlaseng.2005.03.008>
37. Sturtevant, B., Kulkarny, V.A.: The focusing of weak shock waves. *J. Fluid Mech.* **73**(4), 651–671 (1976). <https://doi.org/10.1017/S0022112076001559>
38. Gustafsson, G.: Experiments on shock-wave focusing in an elliptical cavity. *J. Appl. Phys.* **61**(11), 5193–5195 (1987). <https://doi.org/10.1063/1.338300>
39. Apazidis, N.: Focusing of strong shocks in an elliptical cavity. *Shock Waves* **13**(2), 91–101 (2003). <https://doi.org/10.1007/s00193-003-0196-z>
40. Kojima, H., Takahashi, E., Furutani, H.: Breakdown plasma, vortex flow control for laser ignition using a combination of nano- and femto-second lasers. *Opt. Express* **22**(S1), A90 (2014). <https://doi.org/10.1364/oe.22.000a90>
41. Chen, Y.-L., Lewis, J.W.L., Parigger, C.: Spatial and temporal profiles of pulsed laser-induced air plasma emissions. *J. Quant. Spectrosc. Radiat. Transf.* **67**(2), 91–103 (2000). [https://doi.org/10.1016/S0022-4073\(99\)00196-X](https://doi.org/10.1016/S0022-4073(99)00196-X)
42. Holl, R., Grönig, H.: Focusing of weak blast waves. In: Archer, R.D., Milton, B.E. (eds.) *Shock Tubes and Waves: Proceedings of the 14th International Symposium on Shock Tubes and Shock Waves*, pp. 563–570. Sydney Shock Tube Symposium Publishers, Sydney (1983)
43. Sasoh, A.: *Compressible Fluid Dynamics and Shock Waves*. Springer, Singapore (2020). <https://doi.org/10.1007/978-981-15-0504-1>
44. Hu, T.C.J., Glass, I.I.: Blast wave reflection trajectories from a height of burst. *AIAA J.* **24**(4), 607–610 (1986). <https://doi.org/10.2514/3.9314>
45. Amirkhani, M., Taschin, A., Cucini, R., Bartolini, P., Leporini, D., Torre, R.: Polymer thermal and acoustic properties using heterodyne detected transient grating technique. *J. Polym. Sci., Part B: Polym. Phys.* **49**(9), 685–690 (2011). <https://doi.org/10.1002/polb.22233>
46. Gordon, S., McBride, B.J.: Computer program for calculation of complex chemical equilibrium compositions and applications—I. Analysis. NASA Reference Publication 1311 (1994). <https://ntrs.nasa.gov/archive/nasa/casi.ntrs.nasa.gov/19950013764.pdf>
47. Gordon, S., McBride, B.J.: Computer program for calculation of complex chemical equilibrium compositions and applications—II. Users Manual and Program Description. NASA Reference Publication 1311 (1996). <https://ntrs.nasa.gov/archive/nasa/casi.ntrs.nasa.gov/19960044559.pdf>
48. Yageta, J., Shimada, S., Matsuoka, K., Kasahara, J., Matsuo, A.: Combustion wave propagation and detonation initiation in the vicinity of closed-tube end walls. *Proc. Combust. Inst.* **33**(2), 2303–2310 (2011). <https://doi.org/10.1016/j.proci.2010.07.049>
49. Lee, J.H.S.: *The Detonation Phenomenon*. Cambridge University Press, Cambridge (2008). <https://doi.org/10.1017/CBO9780511754708>
50. Keller, J.B.: Multiple shock reflection in corners. *J. Appl. Phys.* **25**(5), 588–590 (2004). <https://doi.org/10.1063/1.1721693>
51. Goodwin, G.B., Houim, R.W., Oran, E.S.: Effect of decreasing blockage ratio on DDT in small channels with obstacles. *Combust. Flame* **173**, 16–26 (2016). <https://doi.org/10.1016/j.combustflame.2016.07.029>
52. Balossier, Y., Virot, F., Melguizo-Gavilanes, J.: Flame acceleration and detonation onset in narrow channels: simultaneous schlieren visualization. *Combust. Flame* **254**, 112833 (2023). <https://doi.org/10.1016/j.combustflame.2023.112833>
53. de Wit, B., Ciccarelli, G., Zhang, F., Murray, S.: Shock reflection detonation initiation studies for pulse detonation engines. *J. Propul. Power* **21**(6), 1117–1125 (2005). <https://doi.org/10.2514/1.14398>
54. Maxwell, B., Pekalski, A., Radulescu, M.: Modelling of the transition of a turbulent shock-flame complex to detonation using the linear eddy model. *Combust. Flame* **192**, 340–357 (2018). <https://doi.org/10.1016/j.combustflame.2018.02.013>
55. Chin, H.M., Chambers, J., Sosa, J., Poludnenko, A., Gamezo, V.N., Ahmed, K.A.: The evolution of pressure gain in turbulent fast flames. *Combust. Flame* **234**, 111641 (2021). <https://doi.org/10.1016/j.combustflame.2021.111641>
56. Ben-Dor, G.: *Shock Wave Reflection Phenomena*. Springer, Heidelberg (2007). <https://doi.org/10.1007/978-3-540-71382-1>
57. Lau-Chapdelaine, S.S.-M., Xiao, Q., Radulescu, M.: Viscous jetting and Mach stem bifurcation in shock reflections: experiments and simulations. *J. Fluid Mech.* **908**, A18 (2021). <https://doi.org/10.1017/jfm.2020.731>

Publisher's Note Springer Nature remains neutral with regard to jurisdictional claims in published maps and institutional affiliations.